studies on intracoronary stents during MRI have been performed (7–10). Some motion has been reported for the Wictor stent, whereas the Palmaz-Schatz stent did not show any displacement in a magnet field. There are theoretic calculations on induction of currents in metallic implants during MRI (11,12). These calculations make noticeable electrical stimulation during standard MRI unlikely. The possibility of inducing electric fields near or in metallic implants has been studied (11–13), and patients with electronic implants such as pacemakers, cardioverter defibrillators, or cochlear implants should not be examined by MRI, although anecdotal reports on studies in patients with cardiac pacemakers exist (14,15). In a pilot study at 1.5 T, no complications within the first 3 days after stent implantation were reported (16).

Heating is induced by the rapidly changing magnetic field, which is able to provoke a local current in electrical conductors and subsequent eddy currents in adjacent materials or tissue. The amount of energy depends on the electrical field and the conductivity of the material. There are two situations relevant to patient studies (17). First, energy is applied on a long device that forms a closed-loop system with the scanner as the "ground" electrode. Under certain circumstances, current induced in this device may use the skin to bridge a small distance. Because the electrical resistance of the skin is high, a significant local temperature increase may occur. The impact on interventional MRI is not fully assessed but may be severe (18–21).

Straight conductant devices may also act like an antenna when aligned to the B_0 field. When the frequency of the field change equals the resonance frequency of the device, a significant increase of local currents and heating is detectable (22). Given a resonant behavior and a maximal radiofrequency (RF) power at 1.5 T/64 MHz by a continuous RF pulse of 1-msec duration, the estimated amount of energy applied would be approximately 0.25 W.

The resonance frequency depends on the length (L) of the device, which can be calculated by the formula

$$L = \frac{c}{2 \times \sqrt{E}}$$

where c is the velocity of light divided by the RF frequency and E is the tissue constant, which is about 100.

As calculated by this formula, the length leading to resonant behavior of a device in a ^{1}H-MRI experiment is 350 mm at 1.0 T/42 MHz and 230 mm at 1.5 T/64 MHz. Thus, it is very unlikely that coronary stents with a length of up to 40 mm will get into resonance during

MRI studies. However, this hypothesis must first be proven, because even small temperature increases induced by local currents may be hazardous in patients with intracoronary stents. For example, a temperature of more than 41°C is able to activate thrombotic processes (23–25) and local activation of coagulation (26–28). Thus, a local increase of temperature by just 4°C may lead to endothelial activation and subsequent intravascular thrombosis or restenosis of the stented vessel. This study addresses the safety of curently used coronary stents with a special focus on temperature changes during ^{1}H-MRI studies in two state-of-the-art clinical systems.

MATERIALS AND METHODS

We assessed 14 different intracoronary stents from 10 manufacturers currently available or tested on the European market (Table 1) in scanners with a field strength of 1.0 T (Siemens Expert, 15 mT/m, Siemens AG, Erlangen, Germany) and 1.5 T (Siemens Vision, 23 mT/m, Siemens AG). The stents were placed into the magnet on a small flexible MR coil (diameter 5 × 10 cm). MRI studies were simulated with application of high energy (clinical worst case MRI, estimated average specific absorption rate of 2.5 W/kg; estimated spatial peak specific absorption rate of 7.5 W/kg) accomplished by using sequences originally dedicated for cardiac MRI; TE, TR,

Table 1

Manufacturer and Type of Stents

- JoStent (3.0 mm diameter, 16 mm length), SITO-Med Germany, Unterschleißheim, Germany
- Palmaz-Schatz stent, Johnson & Johnson Germany, Haan, Germany
- AVE stent, A Vascular Engineering Germany, Neuss, Germany
- NIR stent (3.5 mm diameter, 25 mm length), Boston Scientific Corporation Germany, Ratingen, Germany
- beStent, Wiktor GX stent and Wiktor i stent, Medtronic Germany, Düsseldorf, Germany
- Inflow stent (3.5 mm diameter, 15 mm length) and inflow stent gold (3.5 mm diameter, 15 mm length), Inflow Dynamics Germany, Munich, Germany
- Wallstent, Schneider Germany, Düsseldorf, Germany
- Tenax-Stent, Biotronik Germany, Mönchengladbach, Germany
- Gianturco-Roubin stent (3.5 mm diameter, 20 mm length), Cook Germany, Mönchengladbach, Germany
- Multilink stent (3.0 mm diameter, 15 mm length), Danimed Germany, Isermhagen, Germany

Table 2

MRI Parameters of Sequences Used for the Nonimplanted Stents at 1.0 T

Name	TR	TE	FA	ST	FoV	Pixel	Matrix
T1	108	32	160	20	338	1.56 × 1.32	108 × 256
T2	800	64	180	20	329	1.57 × 1.29	105 × 256
STIR	306	64	180	20	250	1.67 × 1.29	75 × 256
Cine	15	7	30	10	170	0.66 × 0.66	128 × 256
Haste	627	60	160	7	300	1.46 × 1.17	128 × 256
3DA	3.2	1.1	35	60	250	1.95 × 0.98	80 × 256
IRM	340	20		20	300	1.17 × 1.17	256 × 256

TR, repetition time in msec; TE, echo time in msec; FA, flip angle in degrees; ST, slice thickness in mm; FoV, field of view in mm × mm; Pixel, size of 1 pixel in mm × mm; Matrix, size of matrix in mm × mm; 3DA, three-dimensional angiography; IRM, inversion recovery measurement.

flip angle, numbers of acquisition, and slice thickness were set as in clinical routine for cardiac imaging (Table 2). A thermodilution catheter for continuous cardiac output measurements, equipped with a thermistor wire (Baxter 7.5 F thermodilution catheter) was used as "positive control" and folded into a loop to simulate the position inside a patient's pulmonary artery.

After implantation of the stents into the left anterior descending arteries of freshly explanted pig hearts, we repeated the experiments in the 1.5-T system using a head coil to maximize energy transmission (Table 3). The coronary arteries were not perfused to exclude temperature dispersion to record the entire heating effect. The position of the stents in the pig heart was comparable with the most common sites of stenting in patients.

The noncontact temperature measurement of the stents

is based on the quantitative detection of the infrared (IR) radiation emitted by the stents according to Plancks law of radiation. The determination of the absolute stent temperature requires the knowledge of the individual stent emissivity and of the ambient temperature. The metal surface of all stents exhibits low emissivity in a range from 0.1 to 0.3. Thus, all stents were blackened by using graphite spray with an emissivity of $e = 0.93$ to equalize the emissivity of the stents and to avoid ambient IR reflections.

A high-resolution IR imaging system consisting of a PtSi 256 × 256 focal plane array (FPA) was used to detect IR radiation emitted by the stents in a spectral range from 1.9 to 5.4 μm. The thermal resolution is approximately 60 mK, and the frame rate is 50 Hz. Averaging consecutive frames improves the temperature resolution

Table 3

MRI Parameters of Sequences Used for the Implanted Stents at 1.5 T

Name	TR	TE	FA	ST	FoV	Pixel	Matrix
T1	92	32	160	20	197	1.22 × 0.77	81 × 256
T2	142	57	180	20	197	1.31 × 0.77	75 × 256
STIR	400	57	180	20	176	1.17 × 0.69	75 × 256
Cine	2.4	1.2	8	10	300	4.5 × 2.34	50 × 128
Haste 1	520	43	180	8	230	1.54 × 0.9	112 × 256
Haste 2	520	43	180	8	230	1.54 × 0.9	112 × 256
3DA	3.2	1.1	35	60	250	1.95 × 0.98	80 × 256
EPI	1.2	60	90	5	245	3.83 × 1.91	64 × 128

TR, repetion time in msec; TE, echo time in msec; FA, flip angle in degrees; ST, slice thickness in mm; FoV, field of view in mm × mm; Pixel, size of 1 pixel in mm × mm; Matrix, size of matrix in mm × mm; Haste 1, IR Haste with 21 slices; Haste 2, IR Haste with 7 slices; 3DA, three-dimensional angiography; EPI, echo planar imaging.

Table 4

Technical Data of the IR System

Detector type: PtSi Schottky barrier focal plane array
Number of elements: 256 × 256 (65.536).
Pitch: 24 µm
Spectral range: 1.9–5.4 µm
Digital output: 14 bit
Frame rate (image repetition): 50 Hz
Temperature resolution (NETD) (at 29°C): 60 mK (50 Hz)
Dynamic: 14 bit
IR objectives: 30 mm, f/1.2, and 50 mm, f/1.5.
Long-term stability T_{lts}: > 25 hr

to values as low as 10 mK. The technical data of the IR imaging system are summarized in Table 4, and a schematic view of the experimental setup is shown in Fig. 1. The camera head includes the FPA detector and the read-out electronics, which is based on a switched MOS-FET technology. Each individual detector pixel is connected to its own preamplifying MOS-FET transistor. The analog signal on the chip is directly converted in voltage values, which are much more resistant to high magnetic fields than charge values used in conventional CCD-read-out electronics. There are no moving parts in the camera head that can be disturbed by the magnetic field, except for a linear Stirling cooler used for the cooling of the FPA detector down to an operation temperature of 75 K. The data acquired by the IR detector were transmitted by shielded wires to the control unit, which includes the data processing and data storing devices. The control unit was positioned approximately 3 m away from the IR camera head.

The shortest distance between the IR camera head and the MR scanner without interference with the data acqui-
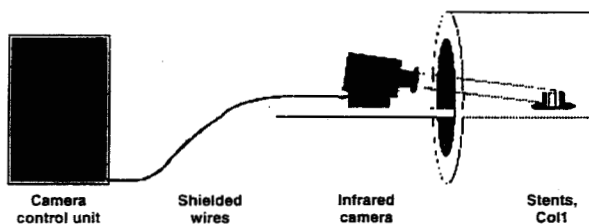
Figure 1. Experimental setup. The IR camera with the tele-lens is positioned in front of the MR scanner at a distance of 0.75 m; the stents under test are in the scanner. The camera control unit and the camera head are separated by a distance of approximately 3 m and are connected by shielded wires.

sition of the camera system by the magnetic field was 75 cm. The distance between the stents under investigation and the camera was approximately 125 cm. The data were recorded just before switching off the gradient system by averaging 100 frames within 2 sec to detect the maximum of temperature increase and to achieve a temperature resolution of approximately 10 mK (29,30). During the studies with the pig hearts, the camera position was optimized to reflect the surface temperature of the vascular wall at the stent locations.

RESULTS

All stents kept their initial position, and the images did not reveal any displacement, suggesting no motion during the scans. There was no significant warming of the stents at 1.0 or 1.5 T. The initial small temperature difference compared with the environment (probably due to the ventilator placed at the other end of the scanner) did not exceed 0.3 K, a value within the standard deviation of the method (Figs. 1 and 2). There were no significant differences for any investigated stents between the temperatures before and after gradients were switched on. The implanted stents did not show significant increases in temperature during the scans and before and after gradients switched on. Small motion of the im-
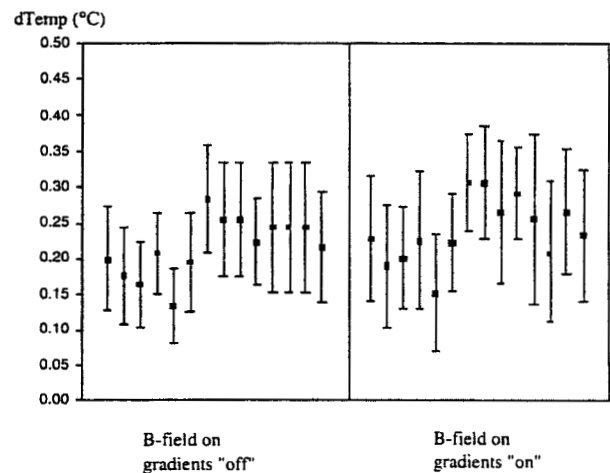
Figure 2. Difference (°C) between the stent temperature and the background temperature with gradient system "off" (left) and "on" (right) in the 14 stents at 1.5 T. Data shown as mean ± SD of 100 measurements within 2 sec. There were no significant differences between gradient system "off" and "on" (all $p \gg 0.05$).
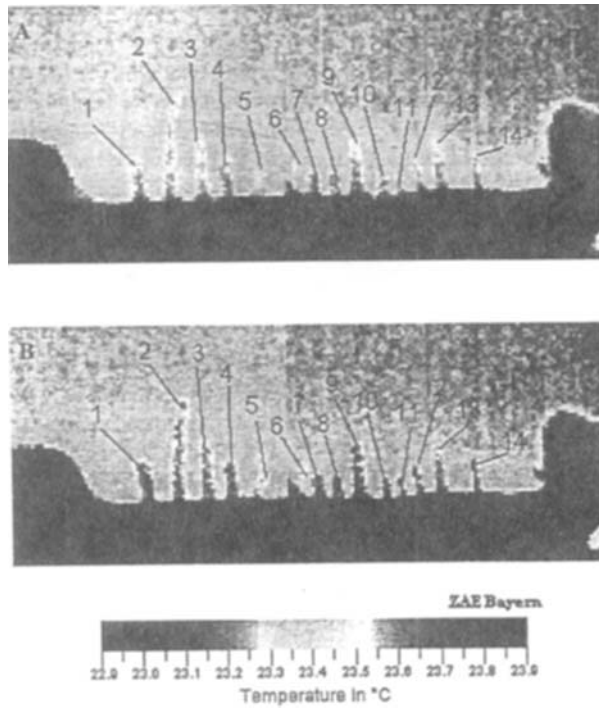
Figure 3. Averaged infrared-image (100 single measurements) of all non-implanted stents at 1.5 T, gradient system "off" (Fig. 2A) and gradient system "on" (Fig. 2B). The stent-surface temperature is shown in gray-scale. The background represents the temperature within the scanner, which is cooled by a ventilation system. Gray-scale in degrees Celsius below. There was no significant difference in temperature (all $p > 0.05$).

planted stents (below visibility) could not be assessed (Fig. 3). The thermodilution catheter showed a local temperature increase of approximately 50°C or 120°F, respectively (Fig. 4) within few seconds after switching the gradients on the 1.5-T. system.

DISCUSSION

In our study we were not able to detect any motion or change of temperature of implantable intracoronary stents during ¹H-MRI studies at 1.0 and 1.5 T. Intracoronary stents are too short for the antenna effect, which is to be expected for objects longer than 23 cm at 1.5 T and 64 MHz. Heating due to a closed-loop system is very unlikely for intracoronary stents, which can only be implanted in straight parts of the coronary arteries and are too short for looping (length up to 40 mm). Even a series
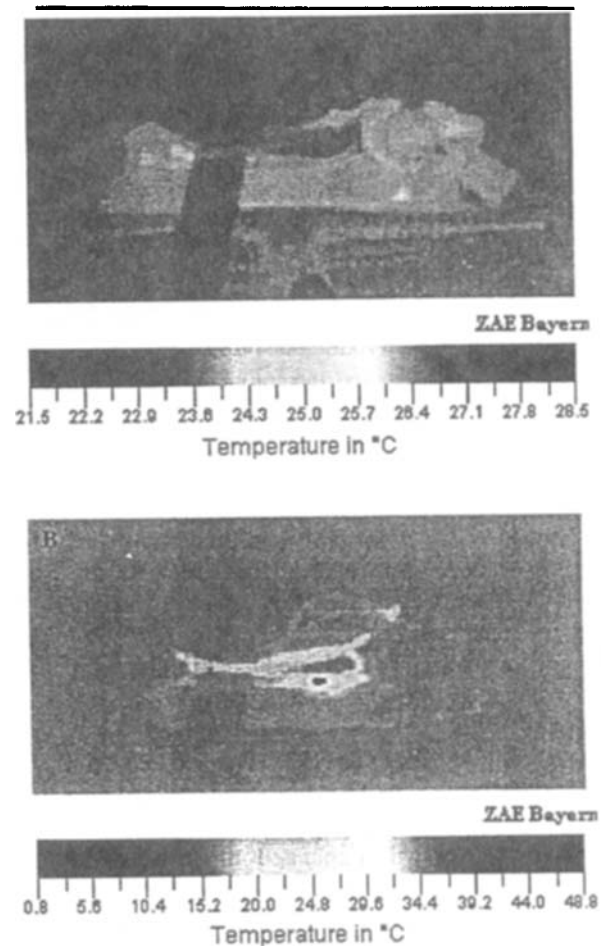
Figure 4. Averaged infrared-image (100 single measurements) of the positive control (thermodilution catheter) at 1.5 T, gradient system "off" (Fig. 3A) and gradient system "on" (Fig. 3B). Gray-scale, see below. Local heating from 24°C to more than 48°C was seen with the gradient system switched "on" within a few seconds (Fig. 3B).

of stents implanted in a row (as sometimes performed in the right coronary artery) would probably not reach a total length of more than 15 cm. There was no significant increase of temperature even in the implanted stents in the no-flow coronaries, which were in the anatomically correct position in the scanner. Thus, a relevant increase of temperature in patients can be excluded, especially because coronary blood flow would further disperse changes of temperature (at least in areas with preserved blood flow).

The thermodilution catheter with the metallic probe inside most likely heated due to the closed loop we formed and emitted a high temperature within a few sec-

onds. The used IR system is able to detect temperature changes of 0.1 mK with a resolution of 256 × 256 pixels; the touch-free measurement of the stents with an acquisition of 50 frames/sec is able to detect the smallest changes in temperature with a standard deviation of 0.1 mK. The measured temperature during the MRI excludes any significant changes in temperature of the investigated stents even under in vitro conditions without the cooling effect of the blood.

There are some limitations to out study. First, the stents were not exactly aligned to the B_0 field. Thus, we may have underestimated the temperature, which could have been reached under ideal alignment. However, this possibility is also unlikely under clinical circumstances. Second, we were not able to assess eddy currents adjacent to the stent. However, the impact of small local currents on tissue in vivo is probably low, although further studies may be needed. Third, we did not calculate the exact amount of energy applied by the MR experiments. However, the calculated results would not have had an impact on our conclusion. The estimated local field strength with a 180-degree high-frequency impulse did not exceed 12 μT.

Our study suggests that ^{1}H-MRI at 1.0 and 1.5 T with gradient systems up to 23 mT/m does not lead to motion or heating of intracoronary stents. We conclude that MRI is safe in patients with implanted intracoronary stents.

REFERENCES

1.   Shellock FG and Morisoli SM. Ex vivo evaluation of ferromagnetism, heating, and artifacts produced by heart valve prostheses exposed to a 1.5-T MR system. *J Magn Reson Imaging*, 1994; 4:756–758.

2.   Soulen RL, Budinger TF and Higgins CB. Magnetic resonance imaging of prosthetic heart valves. *Radiology*, 1985; 154:705–770.

3.   Achenbach S, Moshage W, Diem B, Bieberle T, Schibgilla V and Bachmann K. Effects of magnetic resonance imaging on cardiac pacemakers and electrodes. *Am Heart J*, 1997; 134:467–473.

4.   Leon MB, Popma JJ, Mintz GS, Pichard AD, Satler LF and Kent KM. An overview of US coronary stent trials. *Semin Interv Cardiol*, 1996; 1:247–254.

5.   Chauhan, A, Vu E, Ricci DR, Buller CE, Moscovich MD, Monkman S and Penn IM. Early and intermediate term clinical outcome after multiple coronary stenting. *Heart*, 1998; 79:29–33.

6.   Stone GW, Brodie BR, Griffin JJ, Morice MC, Constantini C, St. Goar FG, Overlie PA, Popma JJ, McDonnell J, Jones D, O'Neill WW and Grines CL. Prospective, multicenter study of the safety and feasibility of primary stenting in acute myocardial infarction: in-hospital and

30-day results of the PAMI stent pilot trial. Primary Angioplasty in Myocardial Infarction Stent Pilot Trial Investigators. *J Am Coll Cardiol*, 1998; 31:23–30.

7.   Scott NA and Pettigrew RI. Absence of movement of coronary stents after placement in a magnetic resonance imaging field. *Am J Cardiol*, 1994; 73:900–901.

8.   Taal BG, Muller SH, Boot H and Koops. Potential risks and artifacts of magnetic resonance imaging of self-expandable esophageal stents. *Gastrointest Endosc*, 1997; 46:424–429.

9.   Teitelbaum GP, Raney M, Carvlin MJ, Matsumoto AH and Barth KH. Evaluation of ferromagnetism and magnetic resonance imaging artifacts of the Strecker tantalum vascular stent. *Cardiovasc Intervent Radiol*, 1989; 12: 125–127.

10. Teitelbaum GP, Bradley WG Jr and Klein BD. MR imaging artifacts, ferromagnetism, and magnetic torque of intravascular filters, stents, and coils. *Radiology*, 1988; 166:657–664.

11. Beuchler DN, Durney CH and Christensen DA. Calculation of electric fields induced near metal implants by magnetic resonance imaging switched-gradient magnetic fields. *Magn Reson Imaging*, 1997; 15:1157–1166.

12. Reilly JP and Diamant AM. Theoretical evaluation of peripheral nerve stimulation during MRI with an implanted spinal fusion stimulator. *Magn Reson Imaging*, 1997; 15: 1145–1156.

13. Shellock FG and Shellock VJ. Vascular access ports and catheters: ex vivo testing of ferromagnetism, heating, and artifacts associated with MR imaging. *Magn Reson Imaging*, 1996; 14:443–447.

14. Lauck G, von Smekal A. Wolke S, et al. Effects of nuclear magnetic resonance imaging on cardiac pacemakers. *Pacing Clin Electrophysiol*, 1995; 18:1549–1555.

15. Gimbel JR, Johnson D, Levine PA and Wilkoff BL. Safe performance of magnetic resonance imaging on five patients with permanent cardiac pacemakers. *Pacing Clin Electrophysiol*, 1996; 19:913–991.

16. Bornstedt A, Helmut H and Nagel E. Intracoronary stents: safety and artefacts during magnetic resonance imaging. *Circulation*, 1997; 96(Suppl. I):I1275–I1528.

17. Jin JM, Chen J, Chew WC, Gan H, Magin RL and Dimbylow PJ. Computation of electromagnetic fields for high-frequency magnetic resonance imaging applications. *Phys Med Biol*, 1996; 41:2719–2738.

18. Bottomley PA and Edelstein WA. Power deposition in whole-body NMR imaging. *Med Phys*, 1981; 8:510–512.

19. Davis PL, Crooks L, Arakawa M, McRee R, Kaufman L and Margulis AR. Potential hazards in NMR imaging: heating effects of changing magnetic fields and RF fields on small metallic implants. *AJR Am J Roentgenol*, 1981; 137:857–860.

20. Budinger TF. Nuclear magnetic resonance (NMR) in vivo studies: known thresholds for health effects. *J. Comput Assist Tomogr*, 1981; 5:800–811.

21. Buchli R, Saner M, Meier D, Boskamp EB and Boesiger P. Increased rf power absorption in MR imaging due to rf

coupling between body coil and surface coil. *Magn Reson Med*, 1989; 9:105–112.

22. Buchli R, Boesiger P and Meier D. Heating effects of metallic implants by MRI examinations. *Magn Reson Med*, 1988; 7:255–261.

23. Tamura K, Kubota K, Kurabayashi H and Shirakura T. Effects of hyperthermal stress on the fibrinolytic system. *Int J Hyperthermia*, 1996; 12:31–36.

24. Hosoi S, Satoh M, Higo K, et al. Modulation of oligosaccharide structure of a pro-urokinase derivative (pro-UK delta GS1) by changing culture conditions of a lymphoblastoid cell line Namalwa KJM-1 adapted to serum-free medium. *Cytotechnology*, 1995; 19:125–135.

25. Krishnan LK and Mathai J. Effect of temperature on functional response of platelet concentrates stored in PVC bags. *Indian J Med Res*, 1997; 105:117–124.

26. Ang C and Dawes J. The effects of hyperthermia on human endothelial monolayers: modulation of thrombotic potential and permeability. *Blood Coagul Fibrinolysis*, 1994; 5:193–199.

27. Bardelle C, Furie B, Furie BC and Gilbert GE. Membrane binding kinetics of factor VIII indicate a complex binding process. *J Biol Chem*, 1993; 268:8815–8824.

28. Chang CH, Lin PJ, Chu Y and Lee YS. Impaired endothelium-dependent relaxation after cardiac global ischemia and reperfusion: role of warm blood cardioplegia. *J Am Coll Cardiol*, 1997; 29:681–687.

29. Schulz MLC. Nonuniformity correction and correctability of infrared focal plane arrays. *Infrared Phys Technol*, 1995;36:763–777.

30. Hierl T, Gross W, Scheurpflug H, Lutz A, Schirl U and Schulz M. Infrared imaging of buried heat sources and material nonuniformities. *Infrared Technol Appl*, 1997; 3061:943–953.